2 μm wavelength range InP-based type-II quantum well photodiodes heterogeneously integrated on silicon photonic integrated circuits

Ruijun Wang,[1,2,*] Stephan Sprengel,[3] Muhammad Muneeb,[1,2] Gerhard Boehm,[3] Roel Baets,[1,2] Markus-Christian Amann,[3] Gunther Roelkens[1,2]

[1] *Photonics Research Group, Ghent University-imec, Sint-Pietersnieuwstraat 41, B-9000 Ghent, Belgium*
[2] *Center for Nano- and Biophotonics (NB-Photonics), Ghent University, Ghent, Belgium*
[3] *Walter Schottky Institut, Technische Universität München, Am Coulombwall 4, 85748 Garching, Germany*
[*] *Ruijun.Wang@intec.ugent.be*

Abstract: The heterogeneous integration of InP-based type-II quantum well photodiodes on silicon photonic integrated circuits for the 2 μm wavelength range is presented. A responsivity of 1.2 A/W at a wavelength of 2.32 μm and 0.6 A/W at 2.4 μm wavelength is demonstrated. The photodiodes have a dark current of 12 nA at −0.5 V at room temperature. The absorbing active region of the integrated photodiodes consists of six periods of a "W"-shaped quantum well, also allowing for laser integration on the same platform.

OCIS codes: (130.0130) Integrated optics; (040.3060) Infrared; (040.0040) Detectors.

References and links

1. L. S. Rothman, I. E. Gordon, Y. Babikov, A. Barbe, D. Chris Benner, P. F. Bernath, M. Birk, L. Bizzocchi, V. Boudon, L. R. Brown, A. Campargue, K. Chance, E. A. Cohen, L. H. Coudert, V. M. Devi, B. J. Drouin, A. Fayt, J.-M. Flaud, R. R. Gamache, J. J. Harrison, J.-M. Hartmann, C. Hill, J. T. Hodges, D. Jacquemart, A. Jolly, J. Lamouroux, R. J. Le Roy, G. Li, D. A. Long, O. M. Lyulin, C. J. Mackie, S. T. Massie, S. Mikhailenko, H. S. P. Müller, O. V. Naumenko, A. V. Nikitin, J. Orphal, V. Perevalov, A. Perrin, E. R. Polovtseva, C. Richard, M. A. H. Smith, E. Starikova, K. Sung, S. Tashkun, J. Tennyson, G. C. Toon, V. G. Tyuterev, and G. Wagner, "The HITRAN2012 molecular spectroscopic database," J. Quant. Spectrosc. Radiat. Transf. **130**, 4–50 (2013).
2. M. N. Petrovich, F. Poletti, J. P. Wooler, A. M. Heidt, N. K. Baddela, Z. Li, D. R. Gray, R. Slavík, F. Parmigiani, N. V. Wheeler, J. R. Hayes, E. Numkam, L. Grűner-Nielsen, B. Pálsdóttir, R. Phelan, B. Kelly, J. O'Carroll, M. Becker, N. MacSuibhne, J. Zhao, F. C. Gunning, A. D. Ellis, P. Petropoulos, S. U. Alam, and D. J. Richardson, "Demonstration of amplified data transmission at 2 μm in a low-loss wide bandwidth hollow core photonic bandgap fiber," Opt. Express **21**(23), 28559–28569 (2013).
3. G. Roelkens, U. Dave, A. Gassenq, N. Hattasan, Chen Hu, B. Kuyken, F. Leo, A. Malik, M. Muneeb, E. Ryckeboer, D. Sanchez, S. Uvin, R. Wang, Z. Hens, R. Baets, Y. Shimura, F. Gencarelli, B. Vincent, R. Loo, J. Van Campenhout, L. Cerutti, J.-B. Rodriguez, E. Tournie, Xia Chen, M. Nedeljkovic, G. Mashanovich, Li Shen, N. Healy, A. C. Peacock, Xiaoping Liu, R. Osgood, and W. M. J. Green, "Silicon-based photonic integration beyond the telecommunication wavelength range," IEEE J. Sel. Top. Quantum Electron. **20**(4), 394–404 (2014).
4. G. Z. Mashanovich, F. Y. Gardes, D. J. Thomson, Youfang Hu, Ke Li, M. Nedeljkovic, J. Soler Penades, A. Z. Khokhar, C. J. Mitchell, S. Stankovic, R. Topley, S. A. Reynolds, Yun Wang, B. Troia, V. M. N. Passaro, C. G. Littlejohns, T. Dominguez Bucio, P. R. Wilson, and G. T. Reed, "Silicon photonic waveguides and devices for near- and mid-IR applications," IEEE J. Sel. Top. Quantum Electron. **21**(4), 8200112 (2015).
5. H. Chen, P. Verheyen, P. De Heyn, G. Lepage, J. De Coster, P. Absil, G. Roelkens, and J. Van Campenhout, "High responsivity low-voltage 28Gb/s Ge p-i-n photodetector with silicon contacts," J. Lightwave Technol. **33**(4), 820–824 (2015).
6. J. J. Ackert, D. J. Thomson, L. Shen, A. C. Peacock, P. E. Jessop, G. T. Reed, G. Z. Mashanovich, and A. P. Knights, "High-speed detection at two micrometres with monolithic silicon photodiodes," Nat. Photonics **9**(6), 393–396 (2015).
7. G. Roelkens, D. Van Thourhout, R. Baets, R. Nötzel, and M. Smit, "Laser emission and photodetection in an InP/InGaAsP layer integrated on and coupled to a Silicon-on-Insulator waveguide circuit," Opt. Express **14**(18), 8154–8159 (2006).
8. G. Roelkens, L. Liu, D. Liang, R. Jones, A. W. Fang, B. R. Koch, and J. E. Bowers, "III-V/silicon photonics for on-chip and intra-chip optical interconnects," Laser Photonics Rev. **4**(6), 751–779 (2010).
9. A. Spott, M. Davenport, J. Peters, J. Bovington, M. J. R. Heck, E. J. Stanton, I. Vurgaftman, J. Meyer, and J. Bowers, "Heterogeneously integrated 2.0 μm CW hybrid silicon lasers at room temperature," Opt. Lett. **40**(7), 1480–1483 (2015).

#248066 Received 18 Aug 2015; revised 29 Sep 2015; accepted 30 Sep 2015; published 2 Oct 2015

10. G. Boehm, M. Grau, O. Dier, K. Windhorn, E. Roenneberg, J. Rosskopf, R. Shau, R. Meyer, M. Ortsiefer, and M. C. Amann, "Growth of InAs- containing quantum wells for InP-based VCSELs emitting at 2.3 μm," J. Cryst. Growth **301-302**, 941–944 (2007).
11. N. Hattasan, A. Gassenq, L. Cerutti, J. B. Rodriguez, E. Tournie, and G. Roelkens, "Heterogeneous integra tion of GaInAsSb p-i-n photodiodes on a silicon-on-insulator waveguide circuit," IEEE Photonics Technol. Lett. **23**(23), 1760–1762 (2011).
12. A. Gassenq, N. Hattasan, L. Cerutti, J. B. Rodriguez, E. Tournié, and G. Roelkens, "Study of evanescently-coupled and grating-assisted GaInAsSb photodiodes integrated on a silicon photonic chip," Opt. Express **20**(11), 11665–11672 (2012).
13. S. Sprengel, G. Veerabathran, A. Andrejew, A. Köninger, G. Boehm, C. Grasse, and M. C. Amann, "InP-based type-II heterostructure lasers for wavelengths up to 2.7 μm," in *SPIE Photonics West, Novel In-Plane Semiconductor Lasers XIV* (SPIE, 2015), paper 9382–29.
14. S. Sprengel, A. Andrejew, F. Federer, G. K. Veerabathran, G. Boehm, and M.-C. Amann, "Continuous wave vertical cavity surface emitting lasers at 2.5 μm with InP-based type-II quantum wells," Appl. Phys. Lett. **106**(15), 151102 (2015).
15. S. Sprengel, C. Grasse, P. Wiecha, A. Andrejew, T. Gruendl, G. Boehm, R. Meyer, and M. C. Amann, "InP-Based Type-II Quantum-Well Lasers and LEDs," IEEE J. Sel. Top. Quantum Electron. **19**(4), 1900909–1900917 (2013).
16. B. Chen and A. L. Holmes, Jr., "Optical gain modeling of InP based InGaAs (N)/GaAsSb type-II quantum wells laser for mid-infrared emission," Opt. Quantum Electron. **45**(2), 127–134 (2013).
17. B. Chen and A. L. Holmes, Jr., "InP-based short-wave infrared and midwave infrared photodiodes using a novel type-II strain-compensated quantum well absorption region," Opt. Lett. **38**(15), 2750–2753 (2013).
18. S. Keyvaninia, M. Muneeb, S. Stanković, P. J. Van Veldhoven, D. Van Thourhout, and G. Roelkens, "Ultra-thin DVS-BCB adhesive bonding of III–V wafers, dies and multiple dies to a patterned silicon-on-insulator substrate," Opt. Mater. Express **3**(1), 35–46 (2013).

1. Introduction

Silicon photonics has been attracting a lot of interest for optical communication applications since it can take advantage of silicon electronics process technology to fabricate integrated photonic devices in high volumes and at low cost. In recent years, the silicon photonics application range has broadened to also include optical sensing. Since many important industrial gases have strong absorption lines in the 2 μm wavelength range [1], and since there is also a strong interest in 2 μm wavelength range optical communication systems [2], there is a need for silicon photonic integrated circuits for the 2 μm wavelength range. Several silicon photonics passive optical functions have already been demonstrated in this wavelength range [3, 4]. Besides passive components, photodiodes are one of the key components required in a photonic integrated circuit. The prevailing method for integrating photodiodes on silicon photonic integrated circuits at telecommunication wavelengths is by hetero-epitaxial growth of germanium [5]. Alternatively, defect engineered silicon can be used for this purpose [6]. The integration of III-V material on silicon photonic ICs by adhesive or molecular bonding is a very efficient technology to integrate active devices such as lasers and amplifiers together with photodiodes on the same silicon photonic IC using a single die-to-wafer bonding step [7]. While there are many demonstrations of InP-based heterogeneously integrated devices for the 1.3/1.55 μm optical communication wavelength range [8], there are very few demonstrations beyond 2 μm wavelength. For the 2 μm wavelength range, GaSb-based type-I and InP-based type-II heterostructures can be used to design active devices. Around 2 μm wavelength also strained quantum wells on InP substrate can be used [9], but the maximum operating wavelength of this structure is limited to about 2.3 μm [10]. Adhesively bonded GaSb-based photodiodes on silicon photonic integrated circuits were demonstrated with a dark current of 1.13 μA at –0.1 V and a responsivity up to 1.4 A/W at 2.29 μm wavelength. In this case an intrinsic GaInAsSb layer was used as the absorbing layer [11, 12]. Compared with GaSb, the InP-based material system uses a cheaper substrate and the related hybrid integration processes are much more mature and are therefore more attractive for integration. Recently, high-performance type-II InP-based edge emitting lasers and vertical cavity surface emitting lasers (VCSEL) were reported with lasing wavelength up to 2.7 μm at room temperature [13, 14]. Therefore, the integration of InP-based type-II heterostructures on silicon-on-insulator (SOI) waveguide circuits is a promising way to realize photonic integrated circuits in the 2 μm wavelength range.

#248066 Received 18 Aug 2015; revised 29 Sep 2015; accepted 30 Sep 2015; published 2 Oct 2015

In this paper, we report the heterogeneous integration of InP-based type-II quantum well photodiodes on a silicon photonic integrated circuit. Adhesive bonding technology using a 100 nm thick Benzocyclobutene (DVS-BCB) layer as bonding agent is used for this purpose. A responsivity of 1.2 A/W at a wavelength of 2.32 µm and 0.6 A/W at 2.4 µm wavelength is demonstrated. The photodiodes have a dark current of 12 nA at –0.5 V at room temperature. The absorbing active region of the integrated photodiodes consists of six periods of a "W"-shaped quantum well, also allowing for laser integration on the same platform.

2. Design and Fabrication

Figure 1 shows the schematic cross section of the InP-based type-II quantum well photodiode integrated on a SOI waveguide. The III-V layer stack is bonded to a SOI waveguide circuit using a 100 nm thick DVS-BCB bonding layer. The III-V mesa is a 150 µm long waveguide, tapered from 1 µm width to 3.5 µm (measured at the top of the mesa). The silicon waveguide underneath is a 400 nm thick tapered (from 6 µm to 3 µm width) rib waveguide etched 180 nm deep. A combination of SiN_x and DVS-BCB is used for mesa passivation.

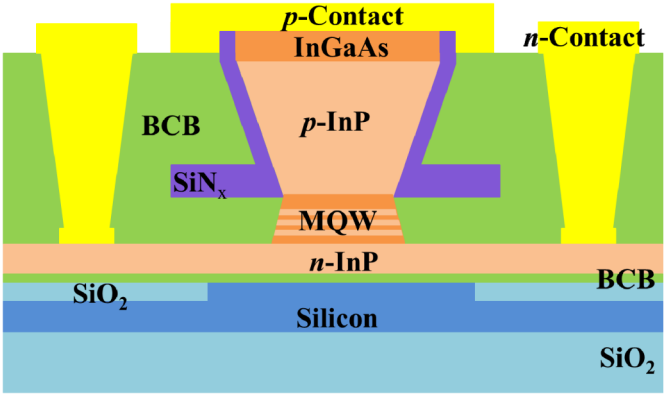

Fig. 1. Schematic drawing of the cross section of the InP-based type-II quantum well photodiodes heterogeneously integrated on a SOI waveguide circuit.

The III-V epitaxial structure has been grown on an *n*-doped (100) InP substrate with a Varian GEN II molecular beam epitaxy (MBE) system. The band structure of the epitaxial stack layer is shown in Fig. 2. The absorbing active region consists of six periods of a "W"-shaped quantum well structure, each separated by 9 nm tensile strained GaAsSb. Every quantum well contains two 2.6 nm InGaAs layers (with a confined electron energy level) and one 2.9 nm GaAsSb layer (with a confined hole energy level), as shown in the inset of Fig. 2. The spatially indirect transition makes that type-II quantum well photodiodes can dectect longer wavelengths than devices based on a type-I heterostructure. The "W"-shaped structure was initially developed to increase laser gain as it improves the overlap between the wave functions of electron and hole states in a type-II quantum well [15]. For photodiodes, this "W"-shaped design thereby also increases the multi-quantum well absorption coefficient. The specific III-V active region design is described in [15], and has been used for the realization of 2.4 µm wavelength lasers. In our III-V epitaxial layer stack, the active region is sandwiched between a 250 nm thick *p*-AlGaAsSb and 130 nm thick *n*-GaAsSb high index layer. The thickness of these two layers was optimized for phase matching between the silicon waveguide and III-V waveguide. The top *p*-cladding layer is 1.5 µm thick *p*-doped InP (~5×10^{17}cm^{-3}). A highly doped InGaAs (~2×10^{20}cm^{-3}) and *n*-doped InP (~2×10^{18}cm^{-3}) is used as *p*-contact and *n*-contact, respectively. Below the *p*-contact layer, a 100 nm InP and 250 nm InGaAs are grown, used as etch stop and sacrificial layer during the substrate removal process.

#248066 Received 18 Aug 2015; revised 29 Sep 2015; accepted 30 Sep 2015; published 2 Oct 2015

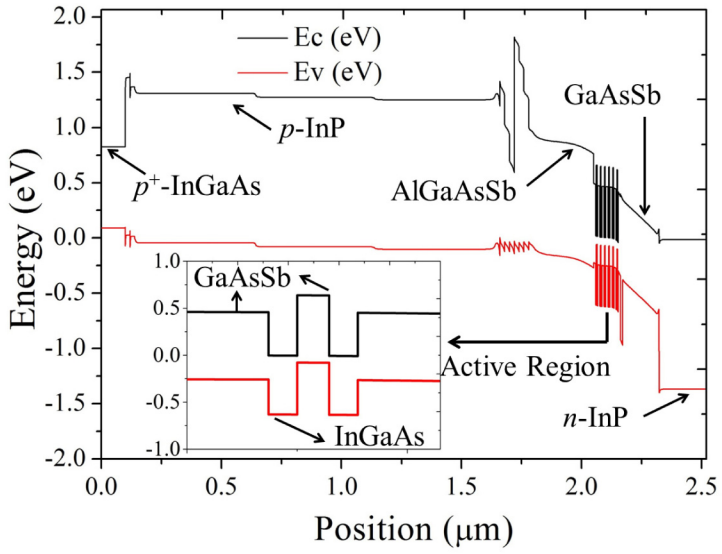

Fig. 2. Band diagram of the type-II quantum well photodiode epitaxial stack under zero bias condition. The inset picture shows the magnification of one period of the a "W"-shaped quantum well structure.

In order to efficiently couple light from the silicon waveguide to the photodiode, a tapered III-V waveguide with a narrow taper tip is designed for adiabatic coupling between the two waveguides. Commercial software (FIMMWAVE) is used for optical device design. The simulated structure is shown in Fig. 3(a). The TE polarized fundamental mode is used (2.35 μm wavelength) in the simulation. As shown in Fig. 3(b) – for a 300nm wide taper tip and 2.5 μm III-V taper end width- the light is confined in the 6 μm wide silicon waveguide in the beginning of the taper and gradually couples to the III-V waveguide when the photodiode mesa becomes wider. The active region absorption is not considered in this simulation. Most of the light will be confined in the III-V waveguide when the III-V waveguide width reaches 0.9 μm. The coupling efficiency of the taper structure is studied for three different taper tip widths: 0.1 μm, 0.3 μm and 0.5 μm, as shown in Fig. 3(c). It can be found that a good coupling can be achieved using a 0.5 μm tip width or less. The typical absorption coefficient of InGaAs/GaAsSb type-II quantum wells in the wavelength range of interest is between 1000 cm^{-1} to 3000 cm^{-1}, as obtained from theoretical calculations and experimental data [16,17], so 150 μm long devices are designed as a compromise between responsivity and dark current. The intensity distribution for the same structure as in Fig. 3(b) when the absorption in the multi-quantum well structure is taken into account is plotted in Fig. 3(d). More than 95% of the light is absorbed in the 150 μm long III-V waveguide using an absorption coefficient of 1000 cm^{-1}.

#248066 Received 18 Aug 2015; revised 29 Sep 2015; accepted 30 Sep 2015; published 2 Oct 2015

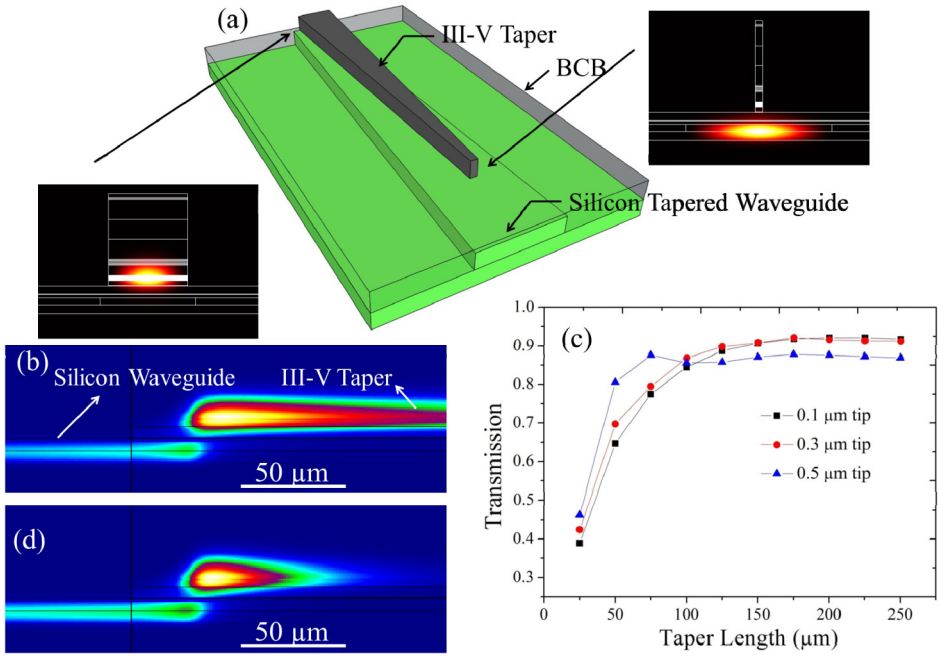

Fig. 3. (a) Schematic of the simulated structure with mode profiles of two cross-sections; (b) Intensity distribution in a longitudinal cross section of the designed taper structure (0.3 um wide III-V taper tip), without considering the active region absorption; (c) mode-to-mode coupling efficiency as a function of taper tip width; (d) Intensity distribution in the designed taper structure taking the active region absorption into account (0.3 um wide III-V taper tip, 1000cm^{-1} quantum well absorption coefficient).

The SOI waveguide fabrication is carried out in imec's CMOS pilot line on a 200 mm SOI wafers with a 400 nm thick silicon device layer (2 μm buried oxide layer thickness). 193 nm deep UV lithography is used for pattern definition after which the silicon rib waveguides are etched 180 nm deep by inductively-coupled plasma (ICP) dry etching. A SiO_2 layer is deposited on the SOI wafer followed by a chemical mechanical polishing (CMP) process to planarize the waveguide circuit down to the silicon device layer. The III-V epitaxial stack is bonded onto the processed SOI by adhesive bonding using a 100 nm thick DVS-BCB bonding layer, the details of which are described in [18]. The InP substrate is removed by a HCl solution using InGaAs as etch stop layer. After the bonding and substrate removal process, the InGaAs/InP sacrificial layer pair is removed and the photodiode mesas are processed on the III-V membrane. The first process is to define a SiN_x hard mask taper with a 1 μm taper tip. Then the InGaAs contact layer is etched by ICP and the *p*-InP cladding layer is etched using a 1:1 HCl:H_2O solution. The anisotropic HCl wet etching of InP creates a negative angle etching when the mesa is oriented along the [01-1] direction, which relaxes the lithographic requirements for the taper tip. For a 1 μm wide taper tip mask on this epitaxial stack, the bottom width of the *p*-InP after HCl etching is around 200 nm wide. Then SiN_x is deposited on the sample as a mask which covers the "V"-shaped p-cladding sidewall, which is used to protect the InP taper structures in the following wet etching process, and passivates the thick *p*-InP cladding layer. The active region is etched by a H_3PO_4: Citric Acid: H_2O_2:H_2O 1:1:20:70 solution, which has a high etching selectivity (~250:1) of GaAsSb to *n*-InP. The isotropic etching of the active region creates an undercut below the SiN_x mask layer. The width of the active region is also around 200 nm in the taper tip section. After the mesa processing, the *n*-InP is etched by diluted HCl to isolate the different devices. Then Ni/Ge/Au is deposited as *n*-contact. Afterwards, DVS-BCB is spin coated on the sample to passivate the devices. After curing at 250°C for 1.5h, the DVS- BCB layer is etched by reactive ion etching

#248066 Received 18 Aug 2015; revised 29 Sep 2015; accepted 30 Sep 2015; published 2 Oct 2015

(RIE) for the opening of the *p*-contact and *n*-contact. In the end, Ti/Au is deposited on the *n*-contact and *p*-contact as probe pad. Figure 4(a) shows a microscope image of the fabricated device. A scanning electron microscope (SEM) image of the device cross section is shown in Fig. 4(b).

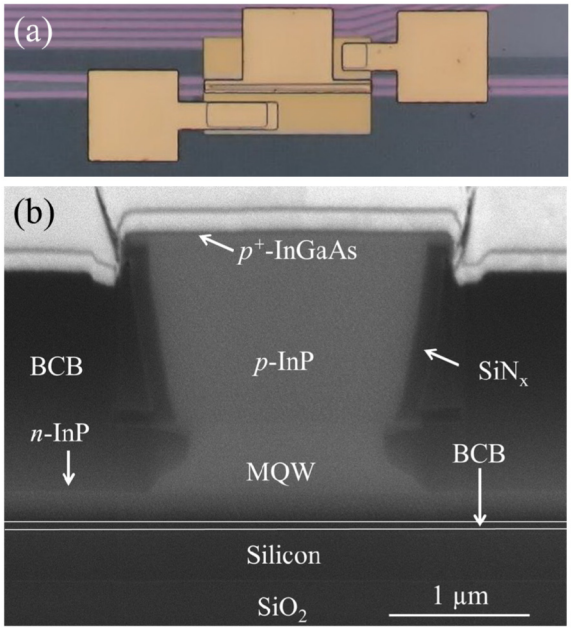

Fig. 4. (a) Microscope image of the heterogeneously integrated type-II quantum well photodiode; (a) SEM image of the cross section of the fabricated devices.

3. Measurement results

The electrical and optical measurements are carried out at room temperature. A Keithley 2400 voltage source is used to apply a bias voltage to the photodiodes during the electrical measurements. In the optical measurements, TE-polarized light from a short-wave infrared (SWIR) tunable laser (IPG Cr:ZnSe solid state laser) is coupled to a standard single mode fiber (SMF-28), which is connected to a 99/1% splitter. The 1% port is connected to an optical spectrum analyzer (Yokogawa AQ6375), which can be used as a power and wavelength reference. 99% of the input power is coupled to a grating coupler to illuminate the silicon waveguide circuit. A 20 μm × 20 μm grating coupler with a period of 1 μm is used to couple TE polarized light from fiber to silicon waveguide for measurement. The measured peak coupling efficiency of the grating coupler is around –9.5dB at 2.35 μm with 150 nm 3dB bandwidth.

#248066 Received 18 Aug 2015; revised 29 Sep 2015; accepted 30 Sep 2015; published 2 Oct 2015

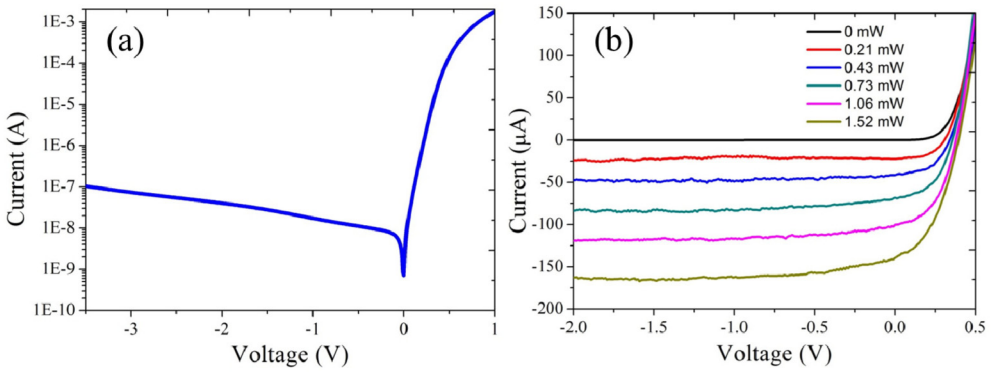

Fig. 5. (a) I-V curve of the photodiode without light input; (b) I-V curve of the photodiode for different fiber-coupled input powers at a wavelength of 2.3 μm.

A typical I-V characteristic of the photodiodes at room temperature is shown in Fig. 5(a). The dark current under reverse bias of 0.5 V is 12 nA (0.17 mA/cm^2). As the reverse bias is increased, the dark current increases gradually but it is still lower than 100 nA at a reverse bias of 3.5 V. This is 3 orders of magnitude lower than the heterogeneous GaSb-based photodiodes previously demonstrated [11], enabling a higher sensitivity. This low dark current can be attributed to the better understood and developed InP processing technology, to the timely BCB passivation of the device, and also to the passivation of the thick *p*-InP cladding layer using SiN_x. Figure 5(b) shows the I-V curve of the devices for different fiber-coupled input powers at a wavelength of 2.3 μm. In the measurement, the photodiodes show good linearity with a fiber-referred responsivity of 0.1 A/W. Considering a coupling efficiency of −11 dB at 2.3 μm wavelength, the corresponding internal responsivity of the photodiodes is around 1.2 A/W, leading to a quantum efficiency of 65%. This high responsivity indicates that the light can be efficiently coupled from the silicon waveguide to the photodiode by using the tapered III-V waveguide.

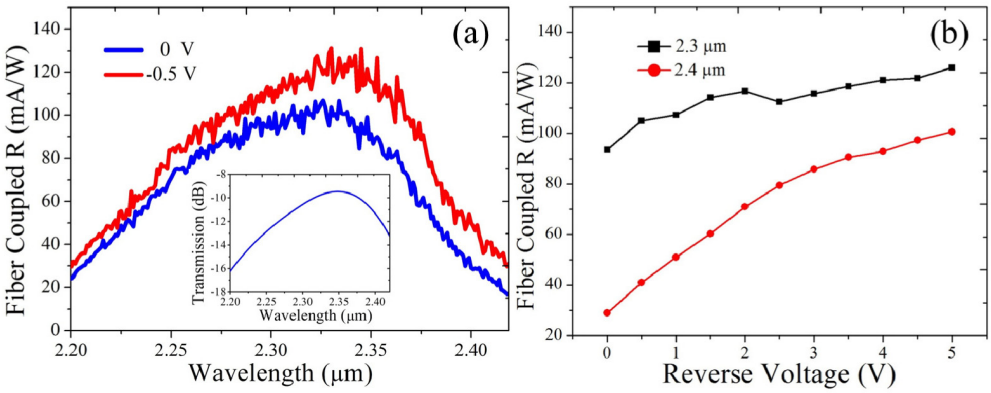

Fig. 6. (a) Dependence of the fiber coupled responsivity (R) on the input laser wavelength under reverse bias of 0 V and 0.5 V, the inset figure shows the referred grating coupler efficiency; (b) responsivity as function of the reverse bias at wavelength of 2.3 μm and 2.4 μm.

Figure 6(a) shows the measured fiber-referred responsivity at 0 V and −0.5 V bias over the 2.2 μm to 2.42 μm wavelength range (the wavelength range limitation of our laser source). The referred grating coupler efficiency is shown in the inset of Fig. 6(a). For the 2.2 to 2.3 μm range the responsivity difference at reverse bias of 0 V and 0.5 V is small. At longer wavelength the optical response becomes strongly dependent on reverse bias. Figure 6(b) depicts the dependence of responsivity on reverse bias (0 to 5 V) at 2.3 μm and 2.4 μm

#248066 Received 18 Aug 2015; revised 29 Sep 2015; accepted 30 Sep 2015; published 2 Oct 2015

wavelength. A much stronger bias dependence can be observed at a wavelength of 2.4 μm. This can be attributed to strong electro-absorption at wavelengths close to the band gap wavelength of the active region. The photodiodes have a waveguide-referred efficiency higher than 0.5 A/W over the 2.2-2.42 μm wavelength range. The measured peak fiber-referred responsivity is 0.12 A/W at 2.32 μm, corresponding to a waveguide-referred efficiency of 1.2 A/W.

4. Conclusion

In this paper, we report for the first time InP-based type-II quantum well photodiodes heterogeneously integrated on an SOI waveguide circuit for operation in the 2.2 to 2.4 μm wavelength range. Simulations and measurements show that an efficient coupling between silicon waveguides and photodiodes can be obtained by using a tapered III-V waveguide. The integrated photodiodes have a low dark current of 12 nA (0.5 V reverse bias) at room temperature and a high waveguide-referred responsivity of 1.2 A/W at a wavelength of 2.32 μm. The epitaxial stack for this photodiode integration can also be used to realize integrated lasers, thereby enabling completely integrated absorption spectroscopy systems on a chip.

Acknowledgements

The author would like to thank S. Verstuyft for metallization processing help and L. Van Landschoot for SEM. This work was supported by the FP7-ERC project MIRACLE and the FP7-ERC-InSpectra.

#248066 Received 18 Aug 2015; revised 29 Sep 2015; accepted 30 Sep 2015; published 2 Oct 2015